EXPERIMENTAL SUMMARY

P. S. WELLS
CERN, CH-1211 Geneva 23, Switzerland

The experimental presentations from the 52nd Rencontres de Moriond session devoted to QCD and High Energy Interactions are summarised. Highlights include Higgs boson measurements from the LHC Run 2, and a first W mass measurement from the LHC. There are various tensions in heavy flavour semileptonic decays which continue to provoke discussion. Top quark and QCD measurements also demand ever more precise theoretical predictions. In direct searches for SUSY particles and other exotic signatures of physics beyond the Standard Model, unfortunately there are no hints of new particles yet. The complicated interplay of phenomena in Heavy Ion Physics is bringing ever better understanding of quark gluon plasma. A rich and diverse programme of measurements is planned for the coming years, adressing the big questions of particle physics.

1 Introduction

At the end of a packed week of talks, the experimental summary can not possibly touch on every result that was shown. The aim is to pick the highlights and hot topics, and to give an impression of the overall status of the field, and the next steps.

The analyses rest on huge investments of effort in accelerator and detector operation and in performance studies. The opening presentation reminded us that last year's target for the LHC was to deliver over 25 fb^{-1} to both ATLAS and CMS, with a peak lumiosity greater than 1.4×10^{34} $\text{cm}^{-2}\text{s}^{-1}$. [1] In practice the integrated luminiosity delivered was 40 fb^{-1} of proton-proton data to the general purpose experiments, together with 1.9 fb^{-1} for LHCb, 13 pb^{-1} for ALICE, and a very successful period of proton-lead running at the end of the year.

2 Higgs Boson Measurements

The combined ATLAS and CMS LHC Run 1 results yield a precise measurement of the Higgs boson mass of $m_H = 125.09 \pm 0.21(\text{stat}) \pm 0.11(\text{syst}) = 125.09 \pm 0.24$ GeV. [2] The overall production rate, divided by the Standard Model (SM) expection is $\mu = \sigma/\sigma_{\text{SM}} = 1.09 \pm 0.11$, in good agreement with the expectation and with 10% precision. [3] The combined production rates for different production modes or different Higgs decay modes are also broadly in agreement with

the SM. Combining the two experiments establishes production by Vector Boson Fusion (VBF) with a significance of 5.4σ (4.6σ expected), and the decay $H \to \tau\tau$ at 5.5σ (5.0σ expected). However, the rate of Higgs boson associated production with a $t\bar{t}$ pair is on the high side, with an observed significance of 4.4σ but only 2.0σ expected. The highest branching ratio should be $H \to b\bar{b}$. This is a difficult decay mode to distinguish from other QCD processes in the dominant gluon-gluon fusion production mode, so analyses rely on associated production with a vector boson or $t\bar{t}$ pair. At present the rate is on the low side, with 2.6σ observed compared to 3.7σ expected.

Results with a larger Run 2 data set at 13 TeV are eagerly awaited to resolve these issues. The golden channels of $H \to \gamma\gamma$ and $H \to ZZ \to \ell\ell\ell\ell$ were presented from ATLAS [4] and CMS. [5] Examples are shown in Figure 1 of fiducial and differential cross-section measurements.

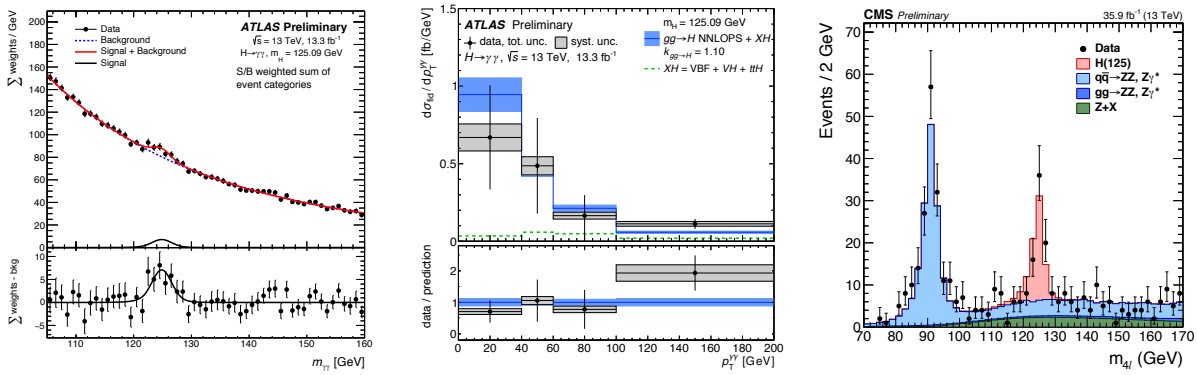

Figure 1 – The diphoton mass spectrum from ATLAS, with a clear excess over background from the Higgs boson at 125 GeV (left), the differential $H \to \gamma\gamma$ cross section as a function of the diphoton transverse momentum for this dataset (centre) and the four lepton mass spectrum from CMS, again showing a clear Higgs boson signal (right)

Differential distributions such as the p_{T} spectrum of the diphoton system will become increasingly sensitive tests of theoretical predictions with higher statistics. Clear diphoton and 4-lepton peaks at 125 GeV are visible. Event categorisations are used to to separate different production modes. The rates of these bosonic final states in different production modes are consistent with expectation at this new centre-of-mass energy of 13 TeV, as shown in Figure 2.

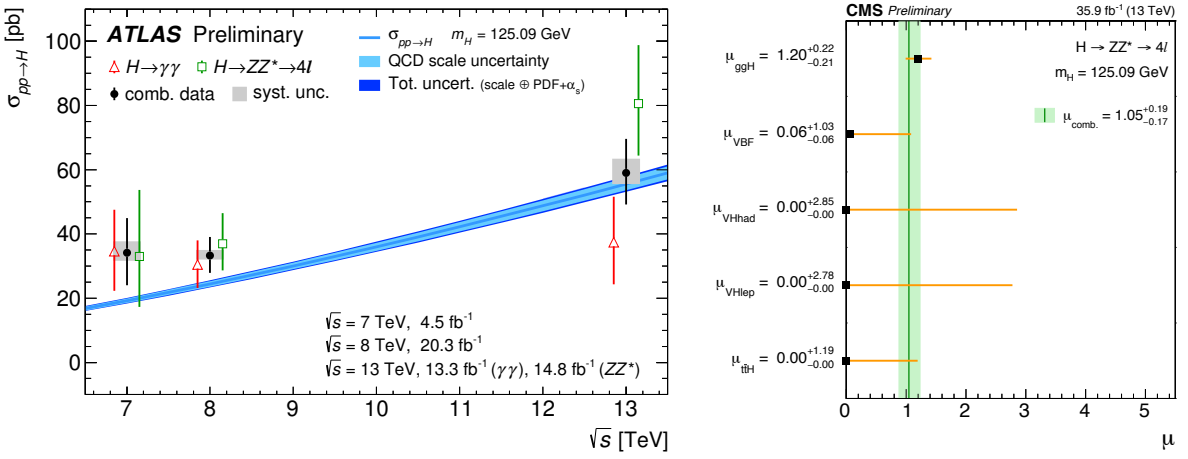

Figure 2 – The combined $\gamma\gamma$ and ZZ Higgs production cross sections from ATLAS as a function of $\sqrt{s}$ (left) and the $H \to ZZ \to 4\ell$ rates compared to the SM expectation in different production modes from CMS (right)

This new CMS 4ℓ sample yields a measurement of the Higgs boson mass of $m_H = 125.26 \pm 0.20(\mathrm{stat}) \pm 0.08(\mathrm{syst})$ GeV. This single measurement is already more precise than the ATLAS and CMS combined Run 1 result. [5]

Table 1: LHC Run 2 results on the rate of $H \to b\bar{b}$, including $t\bar{t}H, H \to b\bar{b}$

	Luminosity [fb^{-1}]	$\mu = \sigma/\sigma_{\rm SM}$
ATLAS ttH	13.2	$2.1^{+1.0}_{-0.9}$
CMSttH	12.9	-0.19 ± 0.80
ATLAS VH	13.2	0.21 ± 0.51
CMS VBF	2.3	$-3.7^{+2.4}_{-2.5}$
ATLAS VBF+γ	12.6	$-3.9^{+2.8}_{-2.7}$

Results with rather limited precision are available for $H \to b\bar{b}$ decays in $t\bar{t}H$, VH and VBF production modes, using up to 13 fb^{-1} of 2016 data.[6] These are listed in Table 1. The tendency for results to be below the SM expectation apparently continues, but more data are obviously needed to draw any firm conclusion.

CMS have new results for $t\bar{t}H$ production in multilepton final states.[7] The decay modes considered are $H \to \tau\tau, WW$ and ZZ, with two same sign leptons, three leptons or four leptons. There is a veto on $H \to ZZ \to 4\ell$ and on hadronic tau decays. Using the full 2016 dataset, this multilepton analysis sees evidence for $t\bar{t}H$ with a significance of 3.3σ (2.5σ expected).

3 Electroweak Measurements

In global fits to the electroweak part of the SM, the prediction of the W mass is more precise than the direct measurement.[8] The Tevatron results are still only available with a partial dataset of 2.2 fb^{-1} (CDF) or 5.3 fb^{-1} (D0), yielding a combined precision of 16 MeV, compared to the combined LEP precision of 33 MeV.[9] The world average W mass from 2013 is 80.385±0.015 GeV. The final Tevatron analysis is in progress, for example there has been a recent improvement in the CDF tracker alignment. Top mass measurements are reported in Section 7.

ATLAS recently published their first W mass measurement using the 7 TeV dataset recorded in 2011.[10,11] The analysis uses $W \to e\nu$ and $W \to \mu\nu$ events, making template fits to the lepton $p_{\rm T}$ or the transverse mass, $m_{\rm T}$, of the $\ell\nu$ system. A sample of $Z \to \ell\ell$ events is also used for calibration; calibration of the leptons and of the hadronic recoil to the W boson is the biggest experimental challenge in this measurement. The multijet background is evaluated from fits in bins of lepton isolation, which are then extrapolated to isolated leptons in the W sample.

With the experimental uncertainties under control, physics modelling uncertainties dominate. These are also controlled by comparison to W or Z data in order to rule out large model variations. For example the $p_{\rm T}$ spectrum is reasonably well modelled with PYTHIA 8 using the AZ tune, and some other models are excluded [10] (see also Section 8). Rapidity distributions and angular variables describing the decay products are reweighted to NNLO calculations, see Figure 3. Angular variables are validated with Z data including the larger 8 TeV sample from 2012.

Separate fits are performed according to lepton charge, lepton flavour (e or μ) and to the $p_{\rm T}$ and $m_{\rm T}$ distributions. The fit results also provide a closure test of the quality of modelling. Two examples are shown in Figure 4. The fit results are consistent, as illustrated in Figure 5. The final result is a weighted average, yielding $m_W = 80370 \pm 7({\rm stat}) \pm 11({\rm exp.syst.}) \pm 14({\rm model})$ MeV, i.e. a combined precision of 19 MeV, equal to the present CDF precision.

The W mass uncertainties are compared in Table 2 [9,10], where the ATLAS uncertainties are taken from Table 11 of Ref.[11] for the combined result. To achieve a 10 MeV total uncertainty, the dominant PDF uncertainties, will have to be reducted to about 5 MeV for the Tevatron results. With the huge samples of W and Z events at the LHC, there is scope to further reduce the experimental systematic uncertainties, and combining measurements with improved calculations

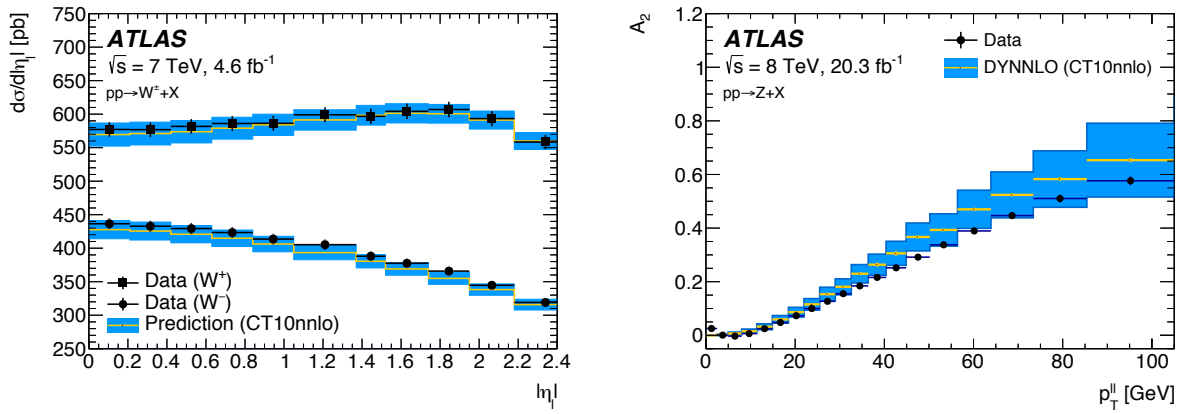

Figure 3 – the W^+ and W^- cross-section as a fuction of the lepton rapidity (left) and the distribution of the angular variable $A2$ for a sample of $Z \to \ell\ell$ events (right)

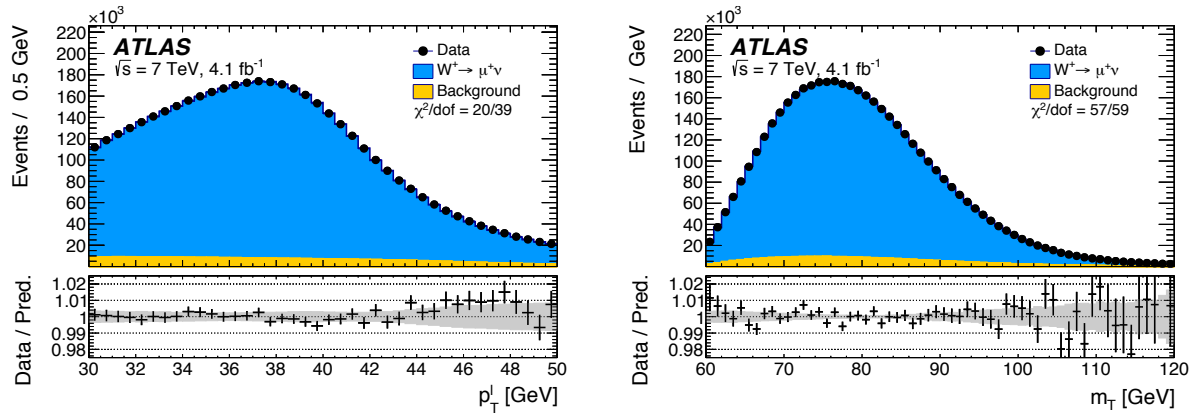

Figure 4 – W mass example fits to the μ^+ p_{T} (left) and m_{T} (right) distributions

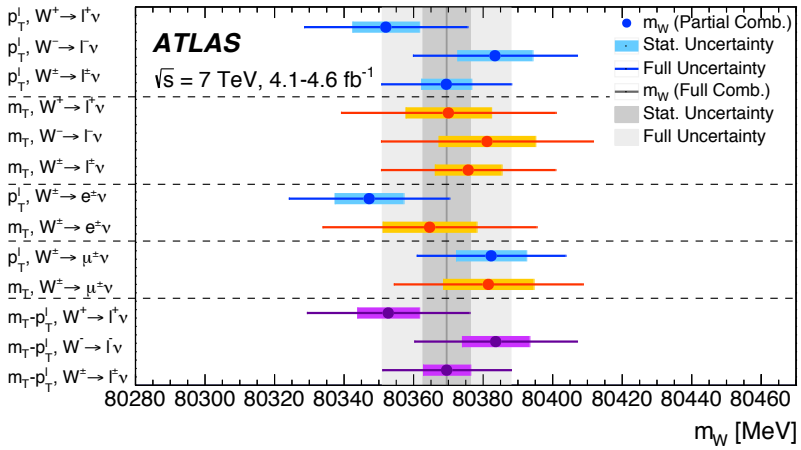

Figure 5 – comparison of W mass results for fits to the lepton p_{T} spectrum or the W transverse mass, for ℓ^+, ℓ^- or combined, and for e, μ or combined

to control the other modelling uncertainties.

Many examples of such measurements were shown. CMS have also measured the angular variables in the Z rest frame as a function of the Z transverse momentum, q_{T}.[12] The forward-backward asymmetry of $Z \to \ell\ell$ decays is of particular interest not only to constrain the proton PDFs, but to measure $\sin^2\theta^{\mathrm{lept}}_{\mathrm{eff}}$.[9, 12, 13] CMS have a new measurement of the forward-backward

Table 2: Systematic uncertainties in the W mass measurements

Uncertainty [MeV]	CDF (2.2fb^{-1})	D0 (4.3fb^{-1})	ATLAS (4.6fb^{-1})
Statistical	12	13	7
Experimental syst	10	18	11
QCD	n/a	n/a	8
PDF	10	11	9
QED	4	7	6
$p_{\mathrm{T}}(W)$	5	2	n/a

asymmetry including forward electrons [12]. LHCb can extend measurements of W and Z bosons into the forward region. They have measurements of the W charge asymmetry and $\sin^2\theta^{\mathrm{lept}}_{\mathrm{eff}}$ from the Z forward-backward asymmetry. [13] The Tevatron measurements of $\sin^2\theta^{\mathrm{lept}}_{\mathrm{eff}}$ are still the most precise from hadron colliders, as shown in Figure 6. As these measurements approach the precision of the LEP and SLD experiments, particular care will be needed to be sure that consistent definitions of $\sin^2\theta^{\mathrm{lept}}_{\mathrm{eff}}$ are used, including QED and QCD corrections.

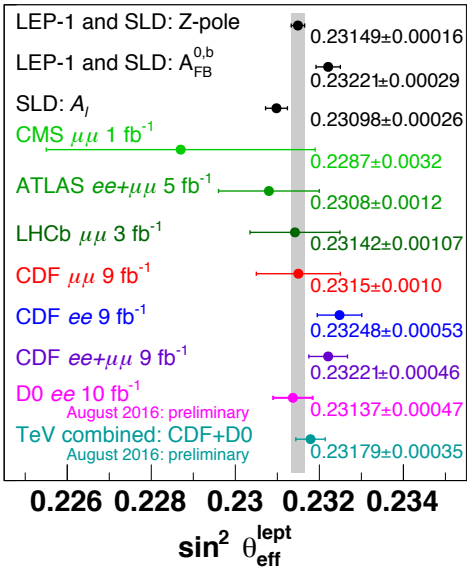

Figure 6 – the most recent combinations of $\sin^2\theta^{\mathrm{lept}}_{\mathrm{eff}}$ measurements from LEP, SLD, the LHC and the Tevatron

Precise measurements at lower energy continue to be relevant for electroweak tests. The hadronic contribution to vacuum polarisation diagrammes is derived from $e^+e^- \to$ hadrons cross-section measurements, as input to calculations of the running of $\alpha(q^2)$ and of the muon $(g-2)$. A new independent evaluation of the running of $\alpha(q^2)$ has been made by the KLOE experiment from the $e^+e^- \to \mu^+\mu^-\gamma$ cross section. [14]

4 Flavour physics

There are numerous tensions in the flavour sector at the $2-3\sigma$ level of significance, and even a small number at about 3.5σ, such as the long established discrepancy between measurement and prediction for the muon $(g-2)$. [15] Three such measurements in semileptonic B decays are discussed below.

In addition, recent results on mixing and CP violation were shown from LHCb, [16] including the final combined LHC Run 1 result for the CKM angle $\gamma = (72.2^{+6.8}_{-7.3})^\circ$. The experiment has also reported the first observation of the decays $\Lambda_b^0 \to p\pi^-\pi^+\pi^-$ and $\Lambda_b^0 \to p\pi^-K^+K^-$. An

asymmetry analysis of these signals yields evidence of CP violation with a significance of 3.3σ, the first evidence for CP violation in baryon decays. Precise measurements of charm mixing have been performed, but here there is no evidence of CPV.

Including some Run 2 data, LHCb have improved their analysis of B_s and $B \to \mu\mu$ decays.[17] The B_s mode is sufficiently precise now to establish the observation in a single experiment, and to make a first evaluation of the $B_s \to \mu\mu$ effective lifetime of $\tau(B_s \to \mu\mu) = 2.04 \pm 0.44 \pm 0.05$ ps.

4.1 Enhanced $B \to D^{(*)}\tau\nu$ rate, $R(D^{(*)})$

The ratio of semileptonic B meson branching ratios to final states with a τ lepton and with a muon, such as $R(D^*) = Br(B \to D^*\tau\nu)/Br(B \to D^*\mu\nu)$, can be precisely predicted in the Standard Model: $R(D^*)_{\rm SM} = 0.252 \pm 0.003$. The ratio is far from unity due to the τ mass. LHCb measured this ratio in 2015 to be $R(D^*) = 0.336 \pm 0.027(\text{stat}) \pm 0.030(\text{syst})$, using $\tau \to \mu\nu\nu$ decays.[18] An analysis using hadronic τ decays is in progress. Measurements from BaBar and Belle are also higher than the expectation. The combined $R(D)$ and $R(D^*)$ results are shown in Figure 7, and are about 3.9σ away from the SM expectation.

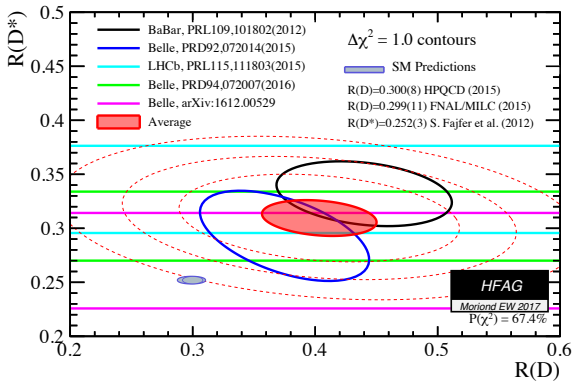

Figure 7 – average measurements of $R(D)$ and $R(D^*)$ from the Heavy Flavour Averaging Group

4.2 Lepton flavour non-universality in $B \to K\mu\mu$ vs. $B \to Kee$, $R(K)$

A second set of lepton flavour universality tests compare the rates of $B \to K\mu\mu$ and $B \to Kee$ decays. In this case the SM expectation is nearly unity. In LHCb, electrons are more difficult to trigger on and to reconstruct, and the result has 1200 signal events in the muon channel, but only 250 events in the electron channel.[18] However, the systematic uncertainties are controlled by using a double ratio, taking the efficiencies from $J/\psi \to \ell\ell$ decays. The measured value is $R(K) = 0.745^{+0.090}_{-0.074} \pm 0.036$, about 2.6σ away from unity. The equivalent $R(K^*)$ and $R(\phi)$ results are in preparation.

4.3 Anomaly in $B \to K * \mu\mu$ angular distributions, P_5'

A third measurement of interest in semileptonic B decays comes from a multiparameter fit to the angular distribution of the decay products in $B^0 \to K^{*0}\mu^+\mu^-$ with $K^{*0} \to K^+\pi^-$.[15] The fit is made as a function of the lepton-pair invariant-mass squared, q^2. It includes a parameter P_5' to describe part of the P-wave contribution, which is expected to be less sensitive to hadronic uncertainties. Measurements from Belle and LHCb tend to be in agreement, and higher than the theoretical prediction in the low q^2 region (Figure 8 left), while the latest results from CMS (Figure 8 centre) and ATLAS (Figure 8 right) are more consistent with theory.[15,19] Note that in this figure, each experiment may not plot the most recent results from the other collaborations. These results concern just one q^2 region of one parameter in a multiparameter fit, so it is very

difficult to assess a combined significance. Nonetheless, it provokes interest and the precision of the measurements will improve with larger data sets.

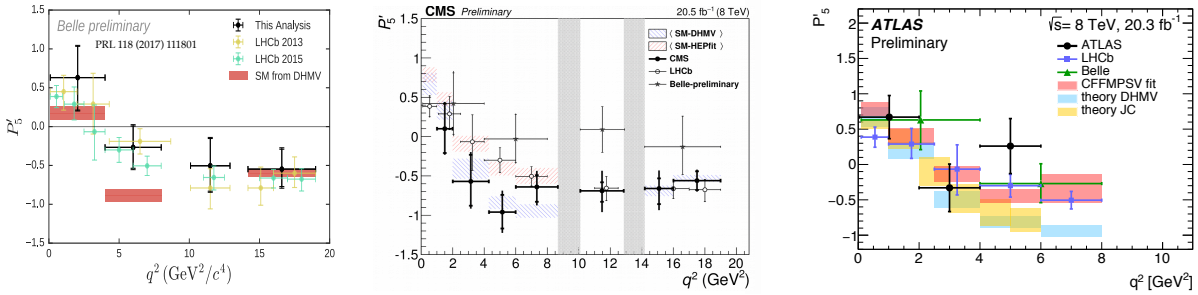

Figure 8 – latest measurements of P_5' from Belle (left), CMS (centre) and ATLAS (right)

5 New and Exotic particles

One of the most striking observations of new states came recently from LHCb [20] in the search for Ω_c^0 excited states in the $\Xi_c^+ K^-$ spectrum, with $\Xi_c^+ \to pK^-\pi^+$. The mass spectrum is shown in Figure 9, showing five new narrow states. The fit includes feed-down from excited Ξ' states, which is consistent with some broader structures around the peaks and the threshold enhancement. This unambiguous experimental data is very hard to match to predictions.

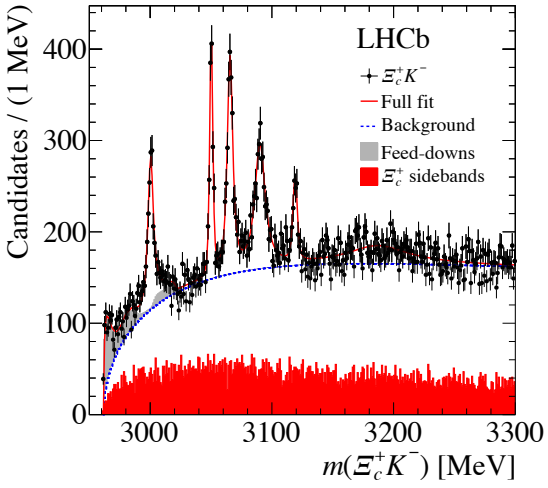

Figure 9 – five new, narrow Ω_c^0 excited states observed by LHCb

This is of course not the only area where predictions lag behind experimental measurements in hadronic spectroscopy. For example, from BESIII, there are unresolved questions of the glueball content of scalar f_0 states, and other other open questions for light hadrons. [21] BESIII has also explored the charmonium-like XYZ states, which bring a curious mixture of states which are predicted and discovered, states which are predicted and undiscovered, and states which were unpredicted, but nevertheless have been observed. [22] The Y states ($J^{PC} = 1^{--}$) can be produced directly in $e^+e^- \to Y$. The X and Z states are accessed by decays of the Y states. For example, the $X(3872)$, which was the first such state to be discovered, has been observed in $e^+e^- \to \gamma X$ with $X \to J/\psi\pi^+\pi^-$. The previously observed $Y(4260)$ has been demonstrated to be inconsistent with a single peak in $e^+e^- \to J/\psi\pi\pi$ with a significance of more than 7σ, and several unpredicted Z states ($J^{PC} = 0^{-+}$) have been established.

Exploration of the equivalent bottomonium-like states continues at the Belle experiment. [23] Two Z_b states hve been observed in $\Upsilon(5S)$ decays. Their branching ratios are dominated by BB^*

and B^*B^* final states: $Br(Z_b(10610) \to BB^* + B^*B^* = 82.6 \pm 2.9 \pm 2.3\%$ and $Br(Z_b(10650) \to B^*B^* = 70.6 \pm 4.9 \pm 4.4\%$.

6 New Phenomena

Many of the presentations on the searches for new phenomena themselves covered a large number of different analyses, making it particularly challenging to summarise what are already a collection of mini-summaries. Unfortunately there is a common theme - no hint of new physics at the energy frontier so far!

Generic searches for dark matter (DM) candidates look for pair produced, neutral, stable DM particles recoiling against a well known particle, creating a single identified final state object and missing transverse energy, known as a mono-X topology. [24] The interpretation is then model dependent. One example of a mono-photon search is shown in Figure 10 (left and centre). A signal would show an excess of events in the signal region with large missing energy. The resulting exclusion depends on the assumed mediator mass, and the coupling of the DM particles to the mediator. Mediator masses up to a TeV are probed. Mono-jet results can be re-expressed as a cross-section for DM-nucleon scattering, and then compared with direct searches for DM particles. The latest such result from CMS is shown in Figure 10 (right). The LHC searches probe a complementary region with lower mass DM particles and smaller cross sections.

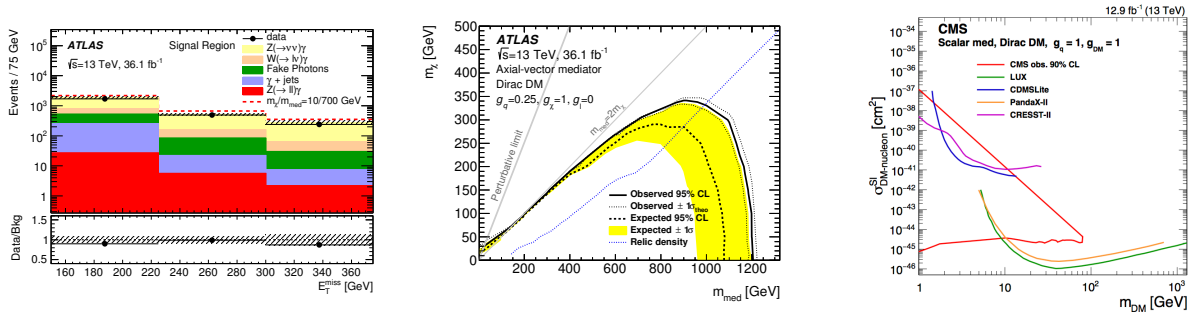

Figure 10 – the $E_{\mathrm{T}}^{\mathrm{miss}}$ distribution from the ATLAS mono-photon search for dark matter (left), the resulting exclusion region for a specific model (centre) and the results of the CMS mono-jet search compared with direct searches (right)

Searches for Supersymmetric partners cover a huge range of final states, and the lightest neutral SUSY particle can be a natural DM candidate. The latest SUSY results from ATLAS and CMS can be grouped into three broad categories. [25, 26]

Strongly produced first and second generation squarks and gluions have the largest production cross sections, so the search reach increases very rapidly with an increased centre-of-mass energy. Pair produced squarks or gluinos and the simple decay chains $\tilde{q} \to q\tilde{\chi}_1^0$ or $\tilde{g} \to qq\tilde{\chi}_1^0$ yield the classic signature with zero leptons, 2–6 jets and large $E_{\mathrm{T}}^{\mathrm{miss}}$. Results with the full 2016 data set exclude squarks up to 1.6 TeV and gluinos up to 2.0 TeV.

Dedicated searches for third generation scalar top quarks are of particular interest because a light stop mass would be sufficient to cancel large corrections to the Higgs boson mass from the top quark, even if the other squarks and gluons are much more massive. Typical final state signatures include top quark decays and result in b-jets, leptons and $E_{\mathrm{T}}^{\mathrm{miss}}$. Particular attention is being paid to searches with close to degenerate stop and top quark masses, with decays such as $\tilde{t}_1 \to bW\tilde{\chi}_1^0$ or $\tilde{t}_1 \to c\tilde{\chi}_1^0$. Two example exclusion plots are shown in Figure 11.

Electroweak production of charginos and neutralinos has a relatively low production cross section, and these searches therefore benefit from the gradual increase of luminosity as Run 2 proceeds. Numerous decay chains including multiple leptons and missing energy are explored, reflecting that different mediators result in different final state flavours and particles.

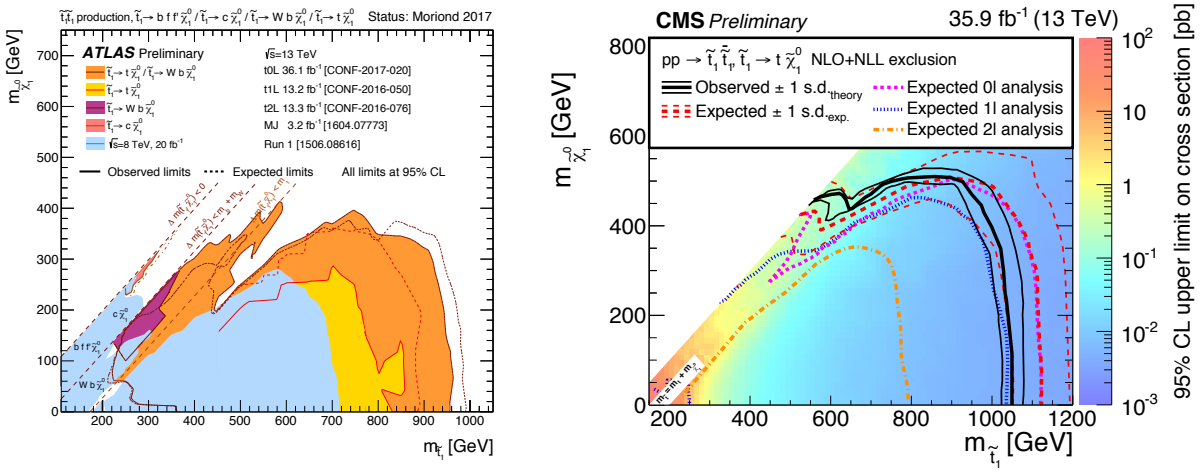

Figure 11 – scalar top quark exclusion limits from ATLAS showing how different final states help to cover the full mass range (left) and an example from CMS of the higher stop mass region (right)

In addition to these three broad categories of searches, SUSY models with compressed spectra and/or R-parity violation can give rise to long lived particles such as displaced jets or tracks which apparently disappear, for example with a decay such as $\tilde{\chi}_1^+ \to \tilde{\chi}_1^0 \pi^+$ where the pion has such low momentum that it is not reconstructed. [24, 25, 26]

It is important to explore these unconventional signatures in order to cover the entire SUSY parameter space and other exotic models. Signatures with boosted objects are also becoming increasingly important as searches explore higher mass regions. [27] The low backgrounds for high mass objects allow hadronic decays to be exploited. Jet substructure variables are used to tag top quark decays and W or Z boson decays. A boosted top quark jet will typically have three subjets, and a mass close to the top quark mass, while a W/Z jet has two subjets and lower mass.

Using boosted topologies, a search for a heavy resonance decaying to a $V = W/Z$ and a Higgs boson by ATLAS shows a small local excess at the 3.3σ level around 3000 GeV but accounting for the look elsewhere effect, the global significance is only 2.2σ. A similar search for $X \to VH \to q\bar{q}b\bar{b}$ by CMS also sees a small excess, but at a lower (and inconsistent) mass around 2600 GeV.

More conventional searches for high mass exotic particles are also continuing. For example, dijet mass and angular distributions studied by ATLAS show no deviations in the full 37 fb^{-1} Run 2 sample to date. [28] The mass distribution is shown in Figure 12 (left). Typical exclusion limits from the dijet studies are: Quantum Black Hole $m(\text{QBH}) > 8.9$ TeV, excited quark $m(q^*) > 6.0$ TeV, excited W, $m(W') > 3.7$ TeV and a contact interaction scale $\Lambda > 13-29$ TeV. Comparable limits from CMS are $m(\text{string}) > 7.7$ TeV, $m(q^*) > 6.0$ TeV and $m(W') > 3.3$ TeV, using wide jets to recover radiation. [29] These observed limits are all close to the expected limits.

Both experiments also look for leptonic decays of exotic particles. Figure 12 (right) shows an example distribution from the CMS search for type III seesaw heavy fermions which could explain the low neutrino masses. The final states are assigned to categories with 3 or 4 leptons, and a limit is set of $m(\Sigma) > 850$ GeV. citeDelRe From leptonic final states, ATLAS also sets limits for $W' \to \ell\nu > 5.1$ TeV, $Z' \to \ell\ell > 3.4-4.1$ TeV and contact interaction scale $\Lambda > 17-25$ TeV. [28]

The Moedel experiment around the LHCb interaction region is something completely different, searching for highly ionising exotic particles such as magnetic monopoles with several approaches: plastic NTD arrays which will be etched and scanned; Timepix radiation monitors; a stack of aluminium bars acting as monopole traps; and the LHCb beam pipe itself, which could also trap monopoles for future analysis. [30] A first scan of aluminium bars has been completed, passing them through a superconducting coil, SQUID, and looking for the induced persistent

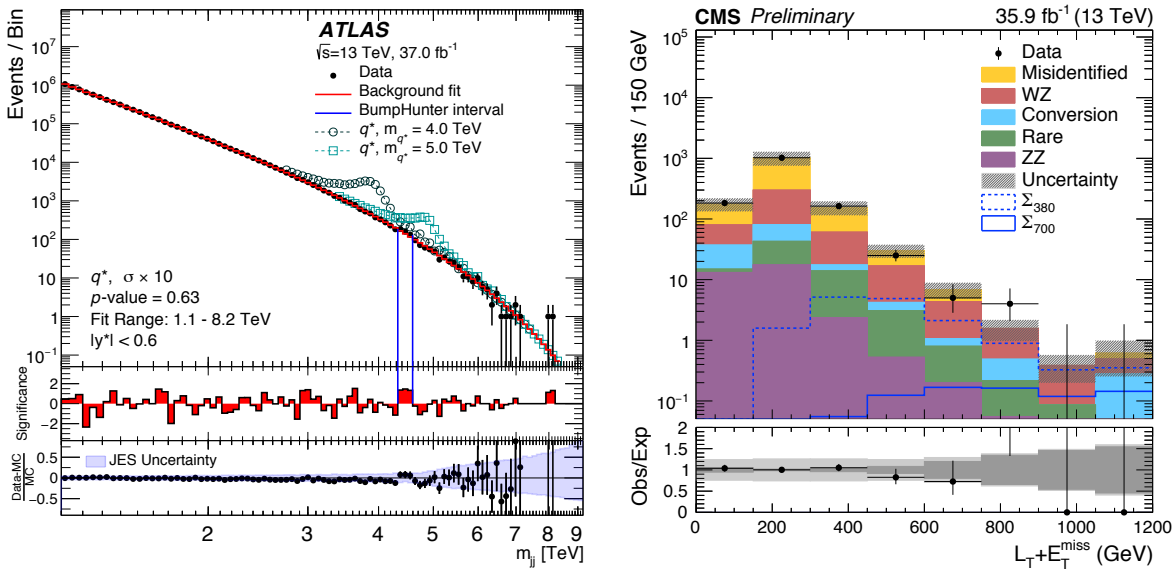

Figure 12 – dijet mass distribution from ATLAS, showing no excess over a smoothly falling distribution (left) and the 3-lepton channel with a lepton pair below the Z-mass from a CMS search for new heavy fermions (right)

current from the passage of a magnetic monopole. Multiple measurements of the samples exclude a magnetic charge of $> 0.5 g_{\mathrm{D}}$ in all of them, where g_{D} is the Dirac magnetic charge. This probes monopole masses in the TeV range for up to $5 g_{\mathrm{D}}$.

7 Top Physics

The latest results on the inclusive $t\bar{t}(+X)$ production cross section almost all date from August 2016 using the 2015 13 TeV dataset. [31] The results are in good agreement with NNLO+NNLL calculations. Differential measurements at 13 TeV reflect modelling issues which were already known from lower centre-of-mass energies, such as problems with the transverse momentum of the $t\bar{t}$ system. First measurements of single top quark production at 13 TeV also use the 2015 data. The $t-$channel and Wt cross sections are in good agreement with expectations. [32]

The latest experimental combinations of the top quark mass measurements using Run 1 data from ATLAS and CMS also date from 2016, and very few Run 2 results have been released so far. [33] The ATLAS average is 172.84 ± 0.70 GeV and the CMS combined value is $172.44 \pm 13 \pm 47$ GeV, compared to the Tevatron combined value of 174.30 ± 0.65 GeV from July 2016. This preliminary result uses the full approximately 10 fb^{-1} from the CDF and D0 experiments and is not expected to change much when it is finalised. [9]

The LHC experiments are exploring novel methods to measure the top mass, for example using the ratio of the mass of the 3-jet top system to the 2-jet W system (ATLAS), looking at the top mass in boosted jets (CMS) or the top mass in single-top events (CMS). These methods help to control uncertainties in the jet energy scale from data, and take advantage of different uncertainties coming from different production mechanisms.

A major concern is to understand how the top quark mass measured from comparisons of a mass distribution to templates created from calculation and/or Monte Carlo simulation relates to the pole mass. This can be addressed by inferring the top quark mass from the measured cross section, which should relate directly to the pole mass. [33, 34] The D0 collaboration have taken this further, to compare the transverse momentum distribution of the top (or anti-top) quark with NNLO predictions as a function of the top quark pole mass. This brings a 25% improvement in precision compared to using the total cross section. [34]

Top quark properties have been explored at the Tevatron and the LHC. Polarisation measurements agree with the SM expectations. Previous forward-backward production asymmetry

measurements at the Tevatron showed some tension with predictions, but the latest measurements from both colliders also agree with the SM. [32, 35]

8 QCD studies

Day five brought the long-awaited QCD session in the Recontres de Moriond: QCD and High Energy Interactions. This began with the latest results from HERA. The $ep \to e'X$ data from H1 and ZEUS provide a unique input to determining the proton PDFs. Although the last collisions were in 2007, a few analyses are still being completed, and comparisons to more modern theoretical calculations can bring improved precision, for example on the measurement of the strong compling constant, α_s, at NNLO from jet production by H1. [36] New heavy quark (c and b) cross section combinations have also been released.

New prompt photon differential cross section measurements are available from ZEUS, CDF and the LHC, where consistency with predictions can be tested in a range of different conditions and exploring the evolution with centre-of-mass energy up to 13 TeV. [36, 37, 38]

The copious jet production at the LHC means that the rates for inclusive jets at the LHC span many more orders of magnitude as a function of p_{T} or E_{T} than direct photon production. Two examples are shown in Figure 13: CMS have extended the measurement of inclusive jet production down to low p_{T}, while ATLAS have released measurements with the 2015 13 TeV data. [38] NLO calculations describe the data well. Some systematic uncertainties cancel when using ratios of production rates at different centre-of-mass energies to compare with predictions. Including the LHC data in PDF fits in addition to HERA data is particularly important to reduce the uncertainty for the high-x gluon distribution. Dijet invariant mass distributions were already shown in Section 6 in the context of searches for exotic particles.

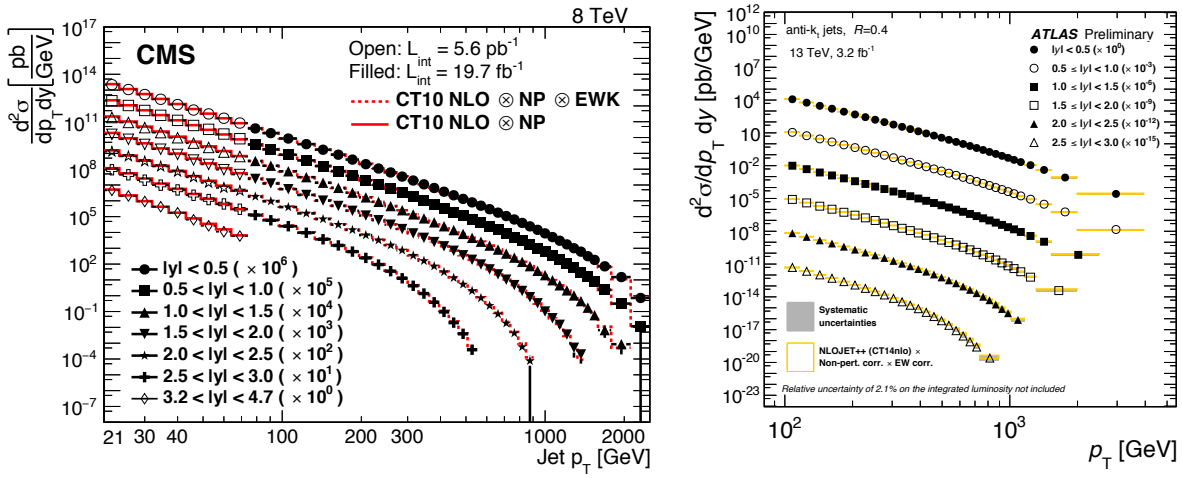

Figure 13 – inclusive jet production from CMS (left) and ATLAS (right)

Inclusive and differential cross section measurements of W and Z boson production are measured by ATLAS and CMS. The distribution of the number of jets and the transverse momentum of the leading jet can be compared with up to NNLO precision. [39] The W/Z plus jet events, and in particular W/Z with heavy flavour jets, are an important background to many searches, and detailed modelling of the shapes of these distributions is critical.

Knowledge of the transverse momentum spectrum of W and Z bosons has a major impact on the W mass measurement, as discussed in Section 3. The situation is unclear, and more detailed exchanges between the experiments and theorists will be needed. One example is shown in Figure 14, where both ATLAS and CMS compare to the prediction from RESBOS (together with other models). [39] ATLAS see reasonable agreement for low $p_{\mathrm{T}}(Z)$, in the full 8 TeV data set. The CMS results come from a special sample with very low pileup. There is some hint of a

similar trend to the ATLAS result for medium p_{T}, but less consistency for the highest p_{T} range plotted.

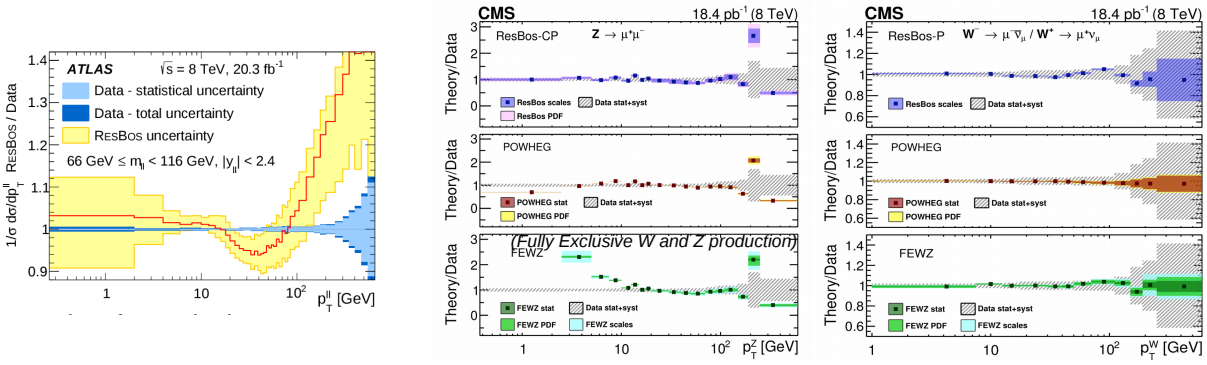

Figure 14 – ratio of theory to data as a function of Z or W p_{T} from ATLAS (left) and CMS (right). Note the different y-axis scales

The rates of multiboson production, including $\gamma\gamma$, $W\gamma$, $Z\gamma$, WW, WZ and ZZ have been measured with the 13 TeV data by ATLAS and CMS and generally agree will with NNLO calculations. [40] These results allow limits to be set on triple and quartic gauge couplings. The high statistics photon-pair sample from the 8 TeV data have been used by ATLAS to make fiducial and differential cross-section measurements as a function of a range of variables chosen so as to be sensitive to different aspects of modelling. [41] For example, the variable a_{T} is the transverse energy of the diphoton system perpendicular to the the thrust of the diphoton system. It is well described by RESBOS at low a_{T}, where infra-red emissions are important. Both RESBOS and DIPHOX are missing higher order α_s corrections, and SHERPA 2.2.1 is in good agreement with data across the full a_{T} range, as shown in Figure 15 (left).

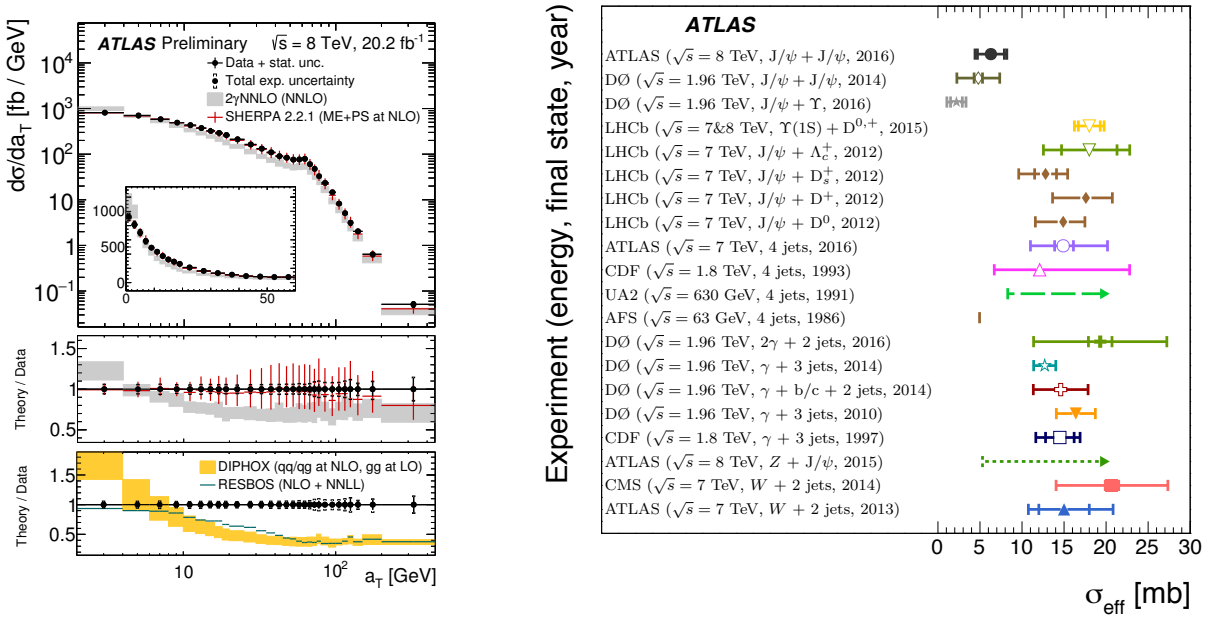

Figure 15 – distribution of a_{T} for diphoton events, compared to predictions (left) and a summary of the effective cross section for double parton scattering for different processes (right)

Soft QCD remains an important area of study at the LHC, in order to describe minimum bias events and the underlying event in hard scattering processes. [42] The rate of double parton scattering, i.e. two hard interactions occuring in the same proton-proton collision, has also been measured for various processes. Assuming no correlations, the cross section σ_{AB} for two

processes, A and B to occur in the same in the same collision depends on the cross sections for the individual processes and an effective cross section $\sigma_{\rm eff}$, defined by

$$\sigma_{AB} = \frac{1}{m} \cdot \frac{\sigma_A \sigma_B}{\sigma_{\rm eff}} \tag{1}$$

New results include: dijet events from the contribution to 4-jet events by ATLAS, ($\sigma_{\rm eff} = 14.9^{+1.2+5.1}_{-1.0-3.8}$ mb); J/ψ pair production from ATLAS ($\sigma_{\rm eff} = 6.3 \pm 1.6 \pm 1.0$ mb); and same sign WW events from CMS ($\sigma_{\rm eff} = 20.7$ mb).[19,42]. The effective cross section for J/ψ pair production tends to be lower than for other processes, as shown in Figure 15 (right).

9 Heavy Ions

The last topic to be covered was heavy ion physics. Proton-proton collisions are already challenging to simulate. New phenomenlogical approaches are needed to deal with hundreds of protons and neutrons interacting in a heavy ion central i.e. head-on collision. In several areas, comparisons are made between proton-proton, proton-ion, peripheral ion-ion (AA) and central ion-ion collisions. Collective effects are starting to be observed even in the highest-energy pp events which mimic effects seen in AA events.

The results presented tested all the stages of evolution of AA collisions, which starts with the production of a quark gluon plasma, where partons move freely in a droplet of hot, dense nuclear matter in thermal equilibrium. As the plasma cools and expands, the geometry of the initial collision transfers to the flow of particles. High $p_{\rm T}$ particles created in the first states of the collision are referred to as hard probes, which also give an insight into the initial state. The hard probes may be modified by interactions in the medium.

At a certain temperature, $T_{\rm chem}$, chemical freeze out occurs, in other words the flavour mixture of the final state particles is fixed. A thermal model does a good job of describing this mixture, and can be tested by comparing the rates of mesons and baryons of different masses or different flavour content.

Although the flavour content is fixed, some excited states may still form in the continuing scattering until the temperature reaches the kinetic freeze out temperature, $T_{\rm kin}$, to produce the final hadrons.

9.1 Flow

Pressure gradients transfer any non-uniform shape of the plasma into a non-uniform $p_{\rm T}$ distribution of the final state particles. Nearby particles should all be moving at the same speed, so their $p_{\rm T}$ depends on their mass. A Fourier analysis of the azimuthal distribution can be made event-by-event. A head-on collision produces a relatively round droplet, while a mid-centrality collision produces an almond shaped droplet, as shown in Figure 16 (left). [43] The integrated flow for charged particles with $0.2 < p_{\rm T} < 30$ GeV shows that v_2 does indeed depend strongly on centrality, peaking at mid-centrality, while the higher components, v_3..., are dominated by fluctuations, see Figure 16 (right). Note that centrality can be viewed as a measure of impact parameter, so a head-on collision has small centrality, and a very peripheral collision has large centrality. The centrality of events is evaluated by some measure which increases monotonically with impact parameter, and the sample then divded up into equal percentiles. The harmonics increase with centre-of-mass energy due to the higher average $p_{\rm T}$ in the higher $\sqrt{s}$ events.

Examining the flow for identified particle types with $p_{\rm T} < 2$ GeV shows a mass ordering consistent with the particles all having the same speed. [43]

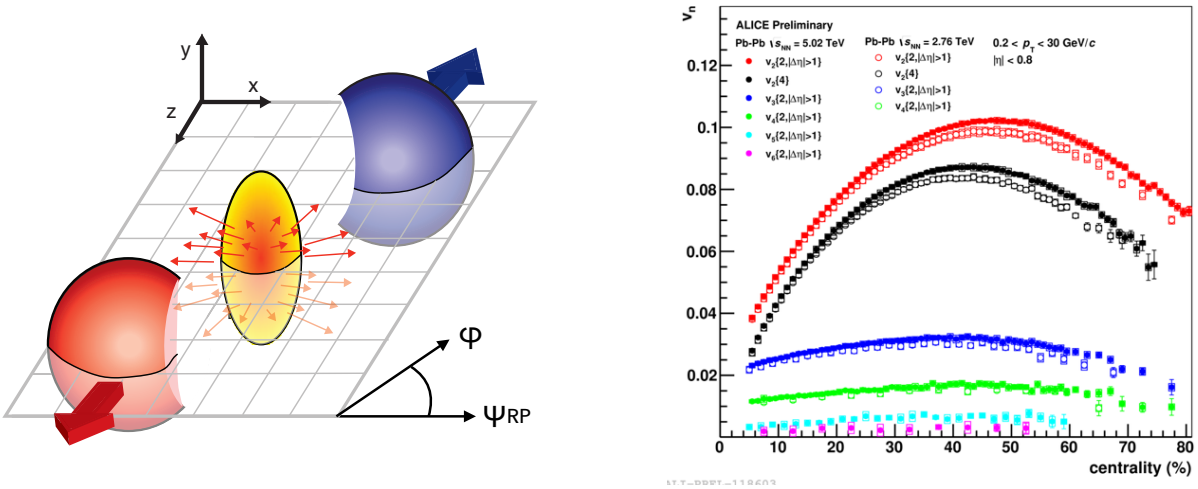

Figure 16 – sketch of a mid-centrality collision (left) and azimuthal Fourier components vs. centrality (right)

9.2 Hard Probes

Hard probes are high p_{T} objects produced early in the collision. The rate is expressed by the nuclear modification factor, R_{AA}, as defined in general by equation 2.

$$R_{AA} = \frac{1}{N_{\mathrm{coll}}} \frac{Y(AA)}{Y(pp)} \tag{2}$$

The rate for a process, Y, in AA collisions is normalised by the rate in pp collisions, scaled by the number of individual nuclear-nuclear collisions, N_{coll}, which is closely related to the number of participating partons, N_{part}.

As shown in Figure 17, R_{AA} for weakly interacting Z bosons is flat - there is no interaction with the medium. However, for jets there is significant suppression of the rate, the so-called jet quenching effect, increasing with the number of participants. [44]

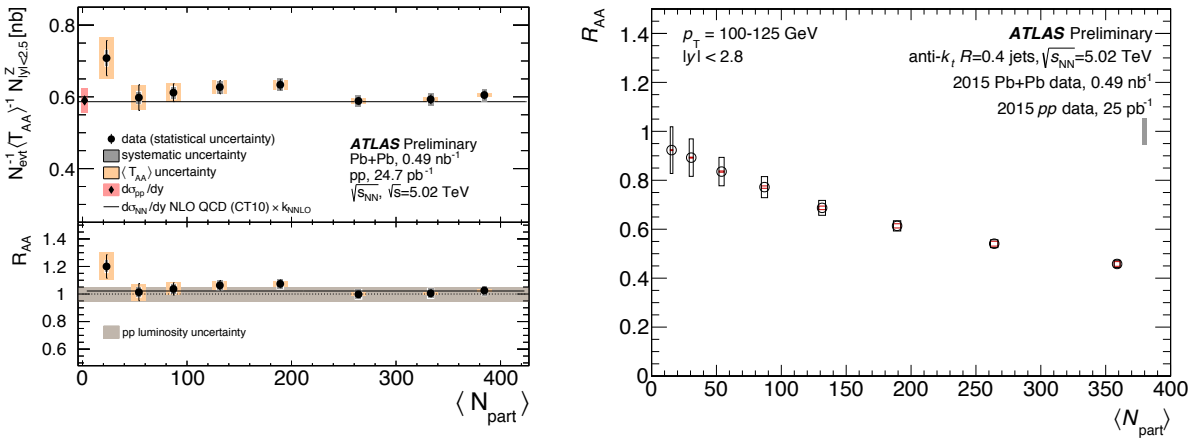

Figure 17 – the normalised event yield and nuclear modification factor, R_{AA} as a function of the number of participating partons for Z bosons (left) and R_{AA} for jets (right)

Another classic signature expected from the formation of quark gluon plasma is the "melting" of quarkonium states due to screening of the $c\bar{c}$ or $b\bar{b}$ pair. Since the different states have different binding energies, the distribution of states is a measure of temperature. [45] The situation is made more complicated because random pairs in the medium can recombine. This is much more likely for $c\bar{c}$ than for $b\bar{b}$. The $\psi(2S)$ has the lowest binding energy, and is suppressed even in the most peripheral collisions. The rate of Υ states is shown in Figure 18 for pp collisions and integrated

over all centralities for Pb+Pb collisions. The $\Upsilon(3S)$ has disappeared in Pb+Pb collisions, and the relative rate of $\Upsilon(2S)$ is reduced.

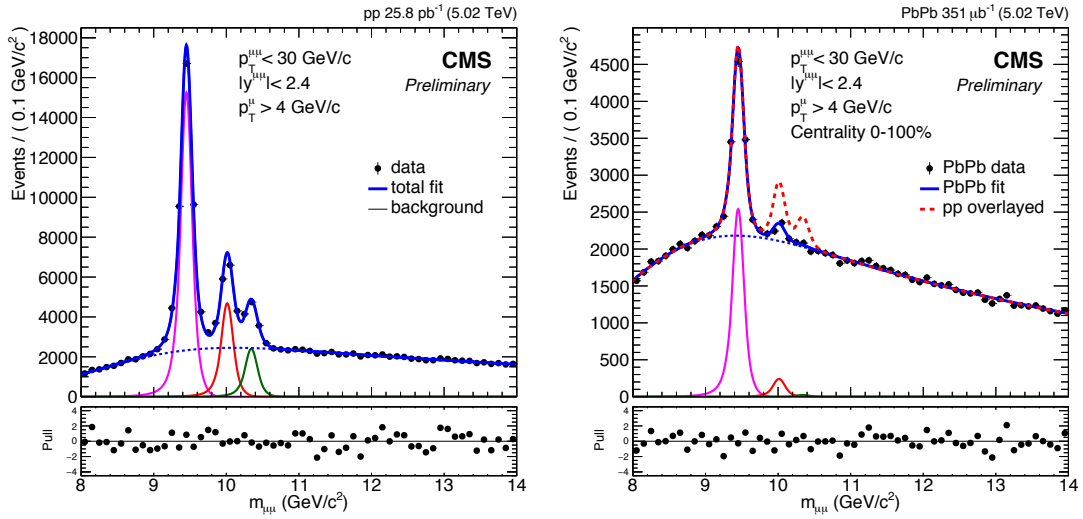

Figure 18 – the $\Upsilon(1S)$, $\Upsilon(2S)$ and $\Upsilon(3S)$ peaks in pp data (left) and Pb+Pb data (right)

The relative rates of J/ψ and $\psi(2S)$ have also been studied in p+Pb by ALICE and LHCb, and in d+Au collisions by PHENIX.[46,47,48] The proton and lead beams in the LHC can circulate in either direction, so that ALICE and LHCb can measure both forward and backward rapdity, where forward is defined as the direction of the outgoing proton. LHCb covers larger $|y|$ than ALICE. Both observe suppression of the J/ψ in the forward direction, and LHCb observes that the $\psi(2S)$ is suppressed both forwards and backwards. PHENIX observe that the $\psi(2S)$ is suppressed relative to the J/ψ.

The STAR collaboration have measured the production of D^0 mesons at high p_{T} in 2014 Au+Au collisions.[49] Thermal production of charm and bottom hadrons is expected to be negligible, so these are also particles produced early in the collision. It is observed that D^0 and pion supression is similar at high p_{T} in central collisions. Measurements of flow show that D^0 mesons also follow the light hadron flow, indicating that they are picked up and move with the other particles.

9.3 Identified particles and soft jets

The ALICE detector has excellent particle identification capability, which is exploited to investigate strangeness enhancement, another classic signature expected from the creation of quark gluon plasma. Figure 19 (left) demonstrates there is a smooth evolution from pp to p+Pb to Pb+Pb collisions.[50] The scaling in pp events depends on the event multiplicity, independent of centre-of-mass energy.[50] The available Monte Carlo generators are unable to reproduce this effect.

Most photons are thermally produced; the small fraction of prompt photons, in particular higher p_{T} photons constituting a hard probe, are not affected by the medium. Thermal photons observed by ALICE and by PHENIX are compared in Figure 19 (right). The two distributions are consistent with a higher effective temperature at the LHC.[51]

The effect of the medium on the shape of low p_{T} jets has been investigated in detail by ALICE.[52] Jets in Pb+Pb events are broader in η than in ϕ, with a dip at the centre, rather than a simple peak. To describe this requires an interplay of jet production and flow in the medium.

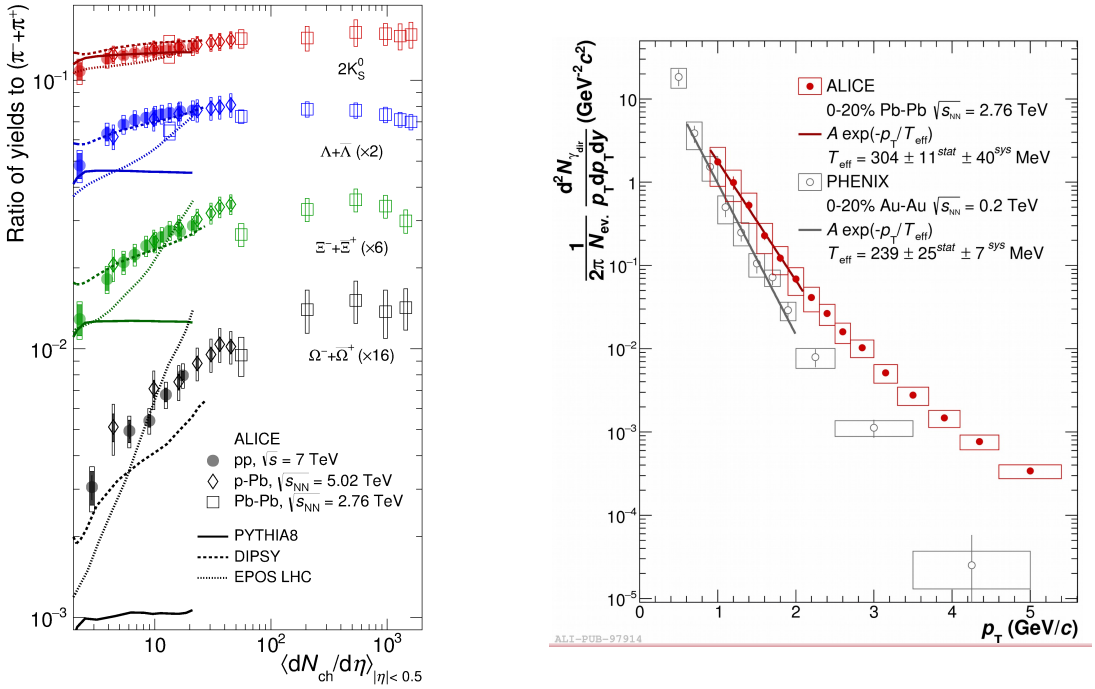

Figure 19 – the rate of strange hadrons normalised to the rate for pions (left) and the rate of thermal photons (right)

9.4 Chiral magnetic effect

The final presentation from the heavy ion session explained the status of investigations of the chiral magnetic effect at RHIC. [53] Measurements of two-particle correlations show a separation between same charge and opposite charge pairs. This could be interpreted as evidence of a QCD topological charge, but there are many background effects to control. It has also been observed that the degree of charge separation also depends on the initial system. Before being able to claim observation of a new phenomenon, more measurements are needed.

10 Future - near and far

The near and far future plans were touched on at many points throughout the conference. For B physics, the LHC will continue and more BESIII data is planned. The Belle II experiment at SuperKEKB should eventually provide 50 times the Belle data sample. [54] Phase I is complete, Phase II will have first collisions at the end of 2017, and Phase III full operation is expected from the end of 2018.

A novel proposal to measure the hadronic contribution to vacuum polarisation directly in $e-\mu$ elastic scattering was shown, [55] and the prospects for precision top and Higgs boson measurements with the first energy stage of CLIC running at 380 GeV have recently been released in an updated baseline document. [56]

The LHC Run 2 will continue in 2017 and 2018 at 13 TeV. [1] A problematic magnet in sector 1-2 was replaced during the end of year technical stop, and the SPS has a new internal beam dump, which will remove a limit on the number of bunches injected in the LHC. The aim for 2017 is to increase the peak instantaneous luminosity to 1.7–1.8 10^{34} cm^{-2}s^{-1} and accumulate 45 fb^{-1} in both 2017 and 2018, with about 50% availability of stable beams during the running period. A 5 TeV pp reference run also has to be scheduled. In long shutdown 2 (LS2), the LHC injectors will be upgraded, allowing 300 fb^{-1} to be delivered before LS3. During LS3 the high luminosity "Phase 2 upgrades" of the accelerator and experiments will take place, aiming to deliver ten times more integrated luminosity in the following decade.

11 Conclusion

This is an exciting time for Higgs boson and electroweak measurements probing the Standard Model more precisely than ever, and exploring electroweak symmetry breaking. The first LHC Run 2 Higgs boson measurements are emerging, with a CMS measurement of the Higgs mass already matching the combined Run 1 precision. The first W mass measurement at the LHC from ATLAS has a precision of 19 MeV. Top quark and QCD measurements also demand ever more precise theoretical predictions. In the area of flavour physics, there are a few anomalies to watch, and hadron spectroscopy measurements are ahead of theory predictions at this stage. In direct searches for SUSY particles and other exotic signatures of physics beyond the Standard Model, unfortunately there are no hints of new particles yet. With the Run 2 data, first and second generation squarks and gluionos are probed up to 2 TeV, and third generation scalar top quarks up to 1 TeV. The complicated interplay of phenomena in Heavy Ion Physics is bringing ever better understanding of quark gluon plasma. A rich and diverse programme of measurements is planned for the coming years, adressing the big questions of particle physics.

Acknowledgments

I would like to thank the organisers for a fascinating conference, and the speakers for the very high quality talks bringing new insights into the present state of our field. It was a fantastic week.

References

1. F. Bordry. LHC status and plans, these proceedings.
2. ATLAS and CMS Collaborations. Combined Measurement of the Higgs Boson Mass in pp Collisions at $\sqrt{s} = 7$ and 8 TeV with the ATLAS and CMS Experiments. *Phys. Rev. Lett.*, 114:191803, 2015.
3. ATLAS and CMS Collaborations. Measurements of the Higgs boson production and decay rates and constraints on its couplings from a combined ATLAS and CMS analysis of the LHC pp collision data at $\sqrt{s} = 7$ and 8 TeV. *JHEP*, 08:045, 2016.
4. R. Nicolaidou. Higgs results from ATLAS, these proceedings.
5. M. Xiao. Higgs results from CMS, these proceedings.
6. W. Murray. Higgs physics with hadronic signatures at ATLAS and CMS, these proceedings.
7. N. Chanon. Search for associated production of Higgs bosons and top quarks in multilepton final states at $\sqrt{s} = 13$ TeV at CMS, these proceedings.
8. M. et al. Baak. The global electroweak fit at NNLO and prospects for the LHC and ILC. *Eur. Phys. J.*, C74:3046, 2014.
9. C. Hays. Electroweak masses at the Tevatron, these proceedings.
10. A. Ruiz-Martinez. Measurement of the W boson mass at ATLAS, these proceedings.
11. ATLAS Collaboration. Measurement of the W-boson mass in pp collisions at $\sqrt{s} = 7$ TeV with the ATLAS detector, arXiv:1701.07240 [hep-ex]. 2017.
12. G. Pasztor. Electroweak measurements in CMS, these proceedings.
13. X. Cid Vidal. Physics with electroweak gauge boson in the forward direction at LHCb, these proceedings.
14. V. De Leo. Measurement of the running of the fine structure constant below 1GeV with the KLOE detector, these proceedings.
15. M. Neubert. Introductory talk of the Heavy Flavour session, these proceedings.
16. J. Fu. Mixing and CP violation in beauty and charm at LHCb, these proceedings.
17. M.-O. Bettler. Rare decays, radiative decays and $b \to sll$ transitions at LHCb, these proceedings.

18. M.-H. Schune. Lepton Flavour Universality tests with B decays at LHCb, these proceedings.
19. M. Galanti. Heavy flavour production and properties at CMS and ATLAS, these proceedings.
20. M. Pappagallo. Hadron spectroscopy and exotic states at LHCb, these proceedings.
21. G. Xu. Light hadron spectroscopy at BESIII, these proceedings.
22. F. Nerling. XYZ at BESIII, these proceedings.
23. P. Krokovny. Bottomonium(-like) states with Belle, these proceedings.
24. L. Soffi. Searches for dark matter and new physics with unconventional signatures at CMS and ATLAS, these proceedings.
25. S. Amoroso. SUSY searches in ATLAS, these proceedings.
26. R. G. Patel. SUSY searches in CMS, these proceedings.
27. G. Brooijmans. Searches with boosted objects at ATLAS and CMS, these proceedings.
28. M. Testa. Search for high mass resonances with ATLAS, these proceedings.
29. D. Del Re. Exotica in CMS, these proceedings.
30. P. Mermod. Latest results from the MoEDAL experiment, these proceedings.
31. L. M. G. Beck. $t\bar{t}(+X)$ pair production at CMS and ATLAS, these proceedings.
32. R. Moles-Valls. Single top production at ATLAS and CMS.
33. J. Monk. Top mass at ATLAS and CMS, these proceedings.
34. B. Hirosky. Top production at the Tevatron, these proceedings.
35. M. S. Soares. Top quark properties at CMS and ATLAS, these proceedings.
36. D. Britzger. High transverse energy jets and photons at HERA, these proceedings.
37. M. Albrow. QCD at the Tevatron, these proceedings.
38. Z. Blenessy. QCD with jets and photons at ATLAS and CMS, these proceedings.
39. M. Wladyslaw Wolter. Inclusive and differential W/Z at ATLAS and CMS, these proceedings.
40. R. Covarelli. Multiboson production at CMS and ATLAS, these proceedings.
41. M. Saimpert. Measurements of integrated and differential cross sections for isolated photon pair production in 8 TeV pp collisions at ATLAS, these proceedings.
42. M. Van De Klundert. Soft QCD at CMS and ATLAS, these proceedings.
43. J. Margutti. Anisotropic flow of charged and identified particles in Pb-Pb collisions at $\sqrt{s}(NN) = 5.02$ TeV with ALICE, these proceedings.
44. M. Rybar. Heavy Ions measurements at ATLAS, these proceedings.
45. C. Lourenco. Heavy Ions measurements at CMS, these proceedings.
46. F. Bossu. Hard probes with pPb and PbPb collisions and fixed target results at LHCb, these proceedings.
47. D. Jouan. Open and hidden heavy flavor production in AA and pA collisions at PHENIX, these proceedings.
48. P. Pillot. Quarkonia and open heavy flavour production with ALICE, these proceedings.
49. R. Ma. Overview of recent heavy-flavor results from STAR, these proceedings.
50. K. Nayak. Multiplicity dependence of identified particle production and strangeness in pp collisions with ALICE, these proceedings.
51. R. Haake. Latest results of photon and jet measurements with ALICE, these proceedings.
52. M. Kofarago. Anomalous evolution of the near-side jet peak shape in Pb-Pb collisions with ALICE, these proceedings.
53. Z. Xu. Chiral magnetic effect at RHIC: where are we?, these proceedings.
54. J. Wiechczynski. Future Belle II experiment at the KEK laboratory, these proceedings.
55. U. Marconi. Measurement of the leading hadronic correction to the muon g-2 in the space-like region, these proceedings.
56. A. Winter. Physics potential of CLIC operation at 380 GeV, these proceedings.